Logic gates on stationary dissipative solitons

Bogdan A. Kochetov,[1] Iaroslavna Vasylieva,[2] Alexander Butrym,[3] and Vladimir R. Tuz[1,2,*]

[1]*State Key Laboratory of Integrated Optoelectronics, College of Electronic Science and Engineering, International Center of Future Science, Jilin University, 2699 Qianjin Street, Changchun 130012, China*

[2]*Institute of Radio Astronomy, National Academy of Sciences of Ukraine, 4 Mystetstv Street, Kharkiv 61002, Ukraine*

[3]*Department of Theoretical Radio Physics, V. N. Karazin Kharkiv National University, 4 Svobody Square, Kharkiv 61022, Ukraine*

(Received 27 March 2019; published 22 May 2019)

Stable dissipative solitons are perfect carries of optical information due to remarkable stability of their waveforms that allows the signal transmission with extremely dense soliton packing without losing the encoded information. Apart from unaffected passing of solitons through a communication network, controllable transformations of soliton waveforms are needed to perform all-optical information processing. In this paper we employ the basic model of dissipative optical solitons in the form of the complex Ginzburg-Landau equation with a potential term to study the interactions between two stationary dissipative solitons under the control influences and use those interactions to implement various logic gates. In particular, we demonstrate NOT, AND, NAND, OR, NOR, XOR, and XNOR gates, where the plain (fundamental soliton) and composite pulses are used to represent the low and high logic levels.

DOI: 10.1103/PhysRevE.99.052214

I. INTRODUCTION

Dissipative optical solitons, localized waves in nonintegrable systems far from equilibrium whose properties depend dramatically on the internal energy balance, were realized at the beginning of 1990s [1,2]. Due to the subsequent theoretical and experimental studies of these solitary waves and unification of their features, the ideas of self-organization, common for the animate and inanimate worlds, were elaborated in the development of the concept of dissipative solitons [3–5]. The theoretical framework for the study of dissipative solitons is based on the complex Ginzburg-Landau equation (CGLE), which accounts for the supply and absorption of energy in the presence of a nonlinear and dispersive (diffractive) environment, crucially important conditions for the development of localized dissipative structures [6–8]. The CGLE admits a few classes of stable solutions representing the rich variety of dissipative solitons and nontrivial behavior of their evolution [9]. In fact, the localized waves governed by the one-dimensional CGLE can evolve as solitons with stationary [10–15], periodically, quasiperiodically, and aperiodically (chaotically) pulsating waveforms [16–18], moving pulses [14], exploding solitons [17–21], solitons with periodic and chaotic spikes of extreme amplitude and short duration [22–24], and multisoliton solutions [25] and in the form of stable dynamic bound states [26]. Remarkably, these different forms of dissipative solitons coexist with each other when the equation coefficients belong to certain regions [14,17–19,27]. Moreover, the basic CGLE can easily be extended to more general models accounting for the impact of such high-order effects as third-order dispersion, fourth-order spectral filtering, self-stepping, and stimulated Raman scattering [28–32] as well as an external control [33,34]. In fact, more specific models have been used to study the turbulentlike intensity and polarization rogue waves in a Raman fiber laser [35], stationary solitary pulses in a dual-core fiber laser [36], the interaction of stationary, oscillatory, and exploding counterpropagating dissipative solitons [37,38], the existence of stable three-dimensional dissipative localized structures in the output of a laser coupled to a distant saturable absorber [39], the emergence and the stability of temporally localized structures in the output of a semiconductor laser passively mode locked by a saturable absorber in the long-cavity regime [40], and dissipative solitons in Bose-Einstein condensates [41–46].

The significant stability of dissipative solitons with respect to the distortion effects allows the soliton passing with very dense pulse packing without losing the encoded information that makes them ideal carriers of information in new optical systems. The development of such systems for performing the all-optical information processing requires robust devices on the dissipative optical solitons, similarly to those for the conservative ones [47]. First of all, the devices can be implemented in the framework of the soliton-soliton interactions. In particular, the AND and OR logic gates based on the self-interactions of bright dissipative polariton solitons have been demonstrated theoretically in [48]. On the other hand, the interactions of dissipative solitons can explicitly be controlled by the externally applied influence. In fact, this control has repeatedly been added to equations governing the soliton dynamics in the form of an external potential. In particular, the diffusion-induced turbulence has been modeled on the basis of the CGLE with an additional term accounting for the global delayed feedback [49] and a gradient force [50]. Spatial localization and dynamical stability of Bose-Einstein condensates of exciton polaritons in microcavities were examined in [43,44]. The nonlinear Schrödinger equation with

*tvr@jlu.edu.cn; tvr@rian.kharkov.ua

a longitudinal defect [51], an external δ potential [52], and a longitudinal potential barrier [53] appear in optical applications for beam splitters. The complex dynamics of dissipative solitons in active bulk media with spatially modulated refractive indices in the form of a sharp potential barrier [54] and umbrella-shaped [55] and radial-azimuthal [56] potentials has been studied on the basis of the one- and two-dimensional cubic-quintic CGLEs.

Accounting for the external magnetic field in nonlinear magneto-optic waveguides leads to another example of controllable optical solitons [57]. Due to the applied magnetic field the time-reversal symmetry is locally broken, which leads to significantly different propagation conditions of counterpropagating dissipative optical solitons whose envelopes are governed by the cubic-quintic CGLE with a potential term [33,34]. Recently, this robust model was successfully used to perform a selective lateral shift within a group of stable noninteracting fundamental dissipative solitons [58], to replicate dissipative solitons and vortices [59,60], and to induce the waveform transitions between different dissipative solitons [61,62].

Since one of the central challenges in the development of promising optical systems based on stable dissipative solitons is getting full control over soliton interactions, we further employ the one-dimensional cubic-quintic CGLE with a potential term to implement logic gates on two different stationary dissipative solitons. Each of these logic gates operates due to a specific control potential applied locally along the propagation distance.

The rest of the paper is organized as follows. In Sec. II we introduce the basic mathematical model of dissipative solitons in the form of a one-dimensional cubic-quintic CGLE with a potential term. This model supports coexistence of two stationary dissipative solitons (plain and composite pulses) with significantly different waveforms and spectra as well as describes their interactions under the control of applied potential. In Sec. III, having applied appropriate control potentials, we demonstrate NOT, AND, NAND, OR, NOR, XOR, and XNOR gates on dissipative solitons, where the plain and composite pulses represent the low and high logic levels. Conclusions and remarks finalize the paper in Sec. IV.

II. MATHEMATICAL MODEL OF CONTROLLABLE DISSIPATIVE SOLITONS

The cubic-quintic CGLE supplemented by a potential term with an explicit coordinate dependence forms the background for simulations of dissipative solitons in many optical applications. In particular, this equation appears in the theory of planar nonlinear magneto-optic waveguides [33,34,58] and describes the evolution of electromagnetic fields in nonlinear optical media with a spatially modulated refractive index [53–56]. Here we adopt the notation used in optics and write the CGLE in the form

$$i\frac{\partial\Psi}{\partial z}+i\delta\Psi+\left(\frac{1}{2}-i\beta\right)\frac{\partial^2\Psi}{\partial x^2}+(1-i\varepsilon)|\Psi|^2\Psi - (\nu-i\mu)|\Psi|^4\Psi+Q(x,z)\Psi=0, \tag{1}$$

where $\Psi(x,z)$ is the complex slowly varying envelope of the transverse x and longitudinal z coordinates. We assume that the coordinates and envelope function are normalized variables. A particular normalization follows from the origin of a physical system. For example, in planar nonlinear magneto-optic waveguides the transverse and longitudinal coordinates are normalized by the effective soliton width w_0 and the Rayleigh length $k_0w_0^2$, respectively [33,34]. In other words, to express the coordinates in natural units one has to use the scaling $x'=w_0x$ and $z'=k_0w_0^2z$, where k_0 is the wave number of the quasimonochromatic optical field centered at the angular frequency ω_0. This normalization provides the natural timescale to estimate the operation time of logic gates demonstrated below.

All coefficients of Eq. (1) are assumed to be positive quantities. This implies that δ and β account for the linear absorption and diffusion, ν stands for the self-defocusing effect due to the quintic nonlinearity, and ε and μ are the cubic gain and quintic loss coefficients, respectively. We note that due to the quintic nonlinear terms, Eq. (1) has numerous stable solutions in the form of both solitons and background [10,63].

The potential $Q(x,z)$ accounts for the influence of linear conservative forces applied externally to control the evolution of the complex envelope $\Psi(x,z)$. Its particular spatial distribution depends on the physical origin of applied forces. For example, in some optical applications the potential $Q(x,z)$ can account for the linear magneto-optic effect [33,34] and spatial modulation of the refractive index [54–56,64,65]. For control purposes it is logical to assume that the potential acts locally along the propagation distance having a finite supporter along the z axis. Without loss of generality, we choose the longitudinal dependence of the potential in the form of a piecewise constant function and write the potential as

$$Q(x,z)=\sum_{i=1}^{N}q_i(x)[h(z-a_i)-h(z-b_i)], \tag{2}$$

where N is the number of control manipulations, $q_i(x)$ is the transverse variation of the potential during the ith control manipulation, $h(\cdot)$ is the Heaviside step function, and $a_i<b_i$ are some points on the z axis at which the potential changes its transverse distribution. The transverse profiles $q_i(x)$, end points a_i and b_i, and number N should be chosen to perform certain control over soliton waveforms. Here they are specified to implement logic gates as discussed later on.

The CGLE admits the existence of a few different attractors at the same values as its coefficients, which means coexistence of different stable dissipative solutions for a given set of parameters [14,17–19,27]. In particular, in wide regions of the parameter space the CGLE allows coexistence of two stable stationary dissipative solitons with different waveforms [14]. One of them is the fundamental soliton, which is also called the plain pulse, while the other one is the so-called composite pulse. Figure 1 shows the typical intensity distributions and normalized power spectra of these two solitons, where the red dotted and blue solid lines indicate the plain and composite pulses, respectively. Moreover, Fig. 1 shows the energies of both solitons calculated in the coordinate space (E_{pp}, E_{cp})

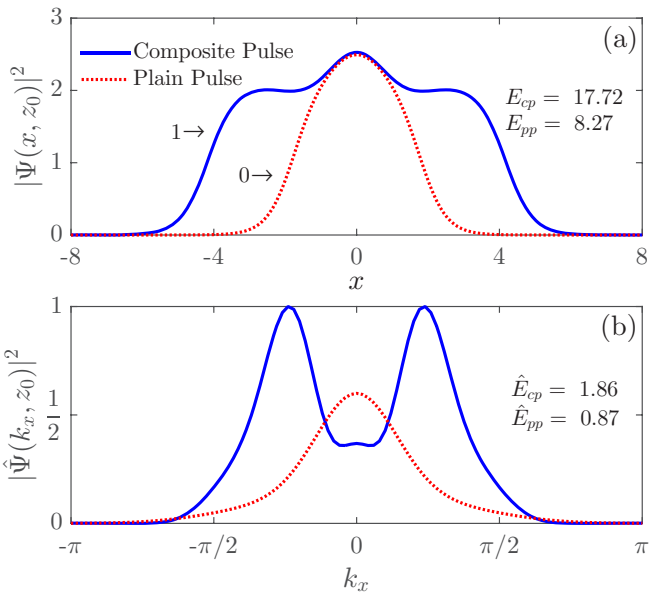

FIG. 1. Two stable stationary dissipative solitons coexisting for the same set of equation coefficients ($\delta = 0.5$, $\beta = 0.5$, $\mu = 1$, $\nu = 0.1$, and $\varepsilon = 2.52$) represent low (0) and high (1) logic levels: (a) intensities and (b) normalized power spectra.

and in the Fourier domain ($\hat{E}_{pp}, \hat{E}_{cp}$), where the subindices stand for the pulse abbreviations. To plot the waveforms of coexisting solitons [Fig. 1(a)] and their spectra [Fig. 1(b)] at some point $z = z_0$ we numerically solve Eq. (1) using the set of coefficients $\delta = 0.5$, $\beta = 0.5$, $\mu = 1$, $\nu = 0.1$, and $\varepsilon = 2.52$ and having applied zero potential, i.e., $Q(x, z) = 0$. We use the same set of numerical values for the coefficients of Eq. (1) here, in all our numerical simulations, which are performed using the exponential time differencing method as well as its Runge-Kutta modification of second- and fourth-order accuracy in the Fourier domain [66]. We apply the fast Fourier transform to the complex amplitude $\Psi(x, z)$ with respect to the transverse coordinate x transforming it to its Fourier amplitude $\hat{\Psi}(k_x, z)$. This imposes the periodic boundary condition

$$\Psi(x, z) = \Psi(x + L_x, z)\ \forall (x, z) \in \mathbb{R} \times [0, +\infty), \qquad (3)$$

with some period $L_x > 0$. Therefore, the computational domain is reduced to the finite rectangular $[-L_x/2, L_x/2] \times [0, L_z]$, where its width $L_x = 100$ is chosen to ensure that all non-negligible parts of the waveforms are within the domain, while its length L_z is chosen to ensure the completion of simulations. Typically, it varies in the range $900 \leqslant L_z \leqslant 3000$. We sample the computational domain with $N_x = 2^{10}$ points along the transverse coordinate x and use the step $\Delta z = 10^{-3}$ to discretize the domain along the longitudinal coordinate z.

Being stationary solutions to Eq. (1), the plain and composite pulses can easily be excited by numerous appropriate waveforms used as initial conditions. In fact, for the specified coefficients of Eq. (1) the plain and composite pulses quickly develop from the initial waveforms $\Psi_{pp}(x)$ and $\Psi_{cp}(x)$, which are respectively defined as

$$\Psi_{pp}(x) = \mathrm{sech}(x), \quad \Psi_{cp}(x) = \exp\left(-\frac{x^2}{25}\right). \qquad (4)$$

III. LOGIC GATES

In this section we demonstrate the implementation of logic gates on dissipative solitons in our simulations based on the numerical analysis of the model (1)–(3). In particular, we exploit two stable stationary solitons admitted by Eq. (1) to represent logic levels. To be specific, we assume that the plain pulse represents the low (0) logic level, while the composite pulse represents the high (1) level. These pulses have different waveforms [Fig. 1(a)] and strictly distinguished spectra [Fig. 1(b)]. Moreover, the plain and composite pulses can also be considered as two isolated stable fixed points (attractors) in an infinite-dimensional phase space of the system (1) [9]. This means that the waveforms and spectra of the pulses are unchangeable along the propagation distance as long as the equation coefficients are fixed and the potential is not applied. In other words, there can be no uncontrollable overlap between the plain and composite pulses that allow them to represent logic levels ideally.

On the other hand, having applied the external potential (2), one can get control over the soliton waveforms, for example, to transit the plain pulse to the composite pulse and to return its waveform [62]. In general, such transitions induced by an external potential can be possible between an arbitrary pair of stable coexisting dissipative solitons if an appropriate control potential is applied [61,62]. We can imagine a particular waveform transition as a forced displacement of a point in the phase space from a basin of attraction of a given attractor to a vicinity of another attractor. Here we further elaborate the ideas of induced waveform transitions [58–62] in the development of controllable interaction between the plain and composite pulses that finally lead us to the implementation of all the logic gates. Below we subsequently demonstrate the most important of them.

A. The NOT gate

We start with the consideration of a NOT gate, which performs the operation of inversion, changing one logic level to the opposite level. In terms of the introduced soliton bits, it changes the plain pulse to the composite pulse [Fig. 2(a)] and the composite pulse to the plain pulse [Fig. 2(b)]. In fact, to complete the description of the NOT gate in the framework of the model (1)–(3) we have to specify the unknown number of manipulations N, start and end points a_i and b_i, and the transverse dependences $q_i(x)$ in the potential (2) used to implement the NOT gate. We should note that these parameters chosen in a different way can lead to multiple implementations of the NOT gate, i.e., there is no unique choice for them. In particular, we assume that each of the transverse dependences $q_i(x)$ is the sum of a few scaled sech(x) functions, which are used as trial functions to approximate the transverse dependence of the potential. For example, the potential (2) suitable to implement the NOT gate contains three control manipulations $N = 3$ with

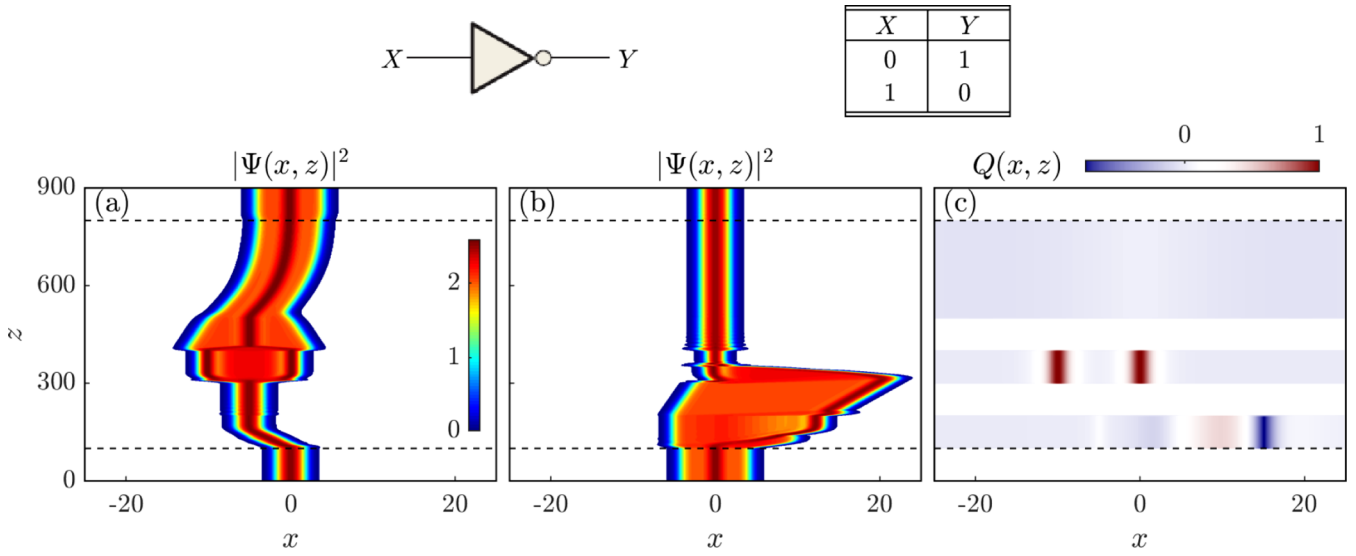

FIG. 2. Truth table for a NOT gate and its implementation on the dissipative soliton bits due to externally applied potential $Q(x, z)$ with the parameters (5): (a) and (b) soliton envelope intensity plots for two-input combinations and (c) plot of control potential.

the parameters

$$
\begin{aligned}
& a_i \in \{100, 300, 500\}, \quad b_i \in \{200, 400, 800\}, \\
& q_1(x) = \frac{1}{10}\mathrm{sech}(2x+10) - \frac{1}{4}\mathrm{sech}\left(\frac{x-2}{2}\right) \\
& \quad + \frac{1}{2}\mathrm{sech}\left(\frac{x-10}{4}\right) - \mathrm{sech}(x-15), \\
& q_2(x) = \mathrm{sech}(x+10) + \mathrm{sech}(x), \\
& q_3 = \frac{1}{20}\left[\mathrm{sech}\left(\frac{x}{5}\right) - \mathrm{sech}\left(\frac{x+19}{10}\right)\right. \\
& \quad \left. - \mathrm{sech}\left(\frac{x-19}{10}\right)\right].
\end{aligned}
\tag{5}
$$

The two-dimensional spatial distribution of the potential (2) with the parameters (5) is plotted in Fig. 2(c), while the evolution of the plain and composite pulses under its influence is shown in Figs. 2(a) and 2(b), respectively, where one can see two-dimensional intensity plots of complex envelopes $|\Psi(x, z)|^2$ of these pulses. More precisely, in Fig. 2(a) we see that the input plain pulse is transited by the potential (2) with (5) to the output composite pulse, while according to Fig. 2(b) we conclude that the same potential transits the input composite pulse to the output plain pulse; thereby potential (2) with the parameters (5) produces the inverted output pulse with respect to the given input pulses. This operation is summarized in the table inserted in Fig. 2, where X and Y stand for the input and output soliton bits, respectively. This table is just the truth table for a NOT gate.

As mentioned above, the potential (2) with (5) inverts the input soliton bits performing three subsequent control stages, which can be clearly seen in Fig. 2(c). At the first stage, the applied potential has the asymmetrical transverse distribution $q_1(x)$, which is chosen to act selectively on the input plain and composite pulses whose waveforms are initially centered at $x = 0$. In fact, it shifts the plain pulse along the negative direction of the x axis [Fig. 2(a)] and changes the composite pulse stretching its waveform along the opposite direction [Fig. 2(b)]. Between the first and second stages, the shifted plain pulse keeps its position unchanged [Fig. 2(a)], while both fronts of the perturbed composite pulse move along the positive direction of the x axis [Fig. 2(b)], which leads to stronger spatial separation of pulses. At the second stage, the two-peaked symmetrical potential $q_2(x)$ transits the shifted plain pulse to the composite pulse [Fig. 2(a)], while the perturbed composite pulse is transited to the plain pulse [Fig. 2(b)]. Between the second and third stages, the pulses released from the potential influence evolve gradually to their unperturbed waveforms. Finally, at the third stage, the relatively weak potential with symmetrical profile $q_3(x)$ is applied to shift the peak of the inverted plain pulse at the initial point $x = 0$ [Fig. 2(a)]. The waveform of the inverted composite pulse was centered around the point $x = 0$ during the second stage. Therefore, its position is not changed during the third stage [Fig. 2(b)]. We should note that the third stage is the longest one because the lateral shifting of the composite pulse [Fig. 2(a)] can only be performed by a weak attractive potential, which slowly shifts the composite pulse without considerable squeezing of its waveform. Otherwise, being attracted by a strong potential, the composite pulse can collapse to the plain pulse [62].

B. The AND and NAND gates

Now we consider the implementation of an AND gate with two inputs using the controllable model (1)–(3), which supports the dissipative soliton bits in the form of plain and composite pulses (Fig. 1). The AND gate produces the composite pulse output only when both of the inputs are composite pulses [Fig. 3(d)]. When either of the inputs is a plain pulse, the output is a plain pulse [Figs. 3(a)–3(c)]. In fact, the implementation of the two-input AND gate presented in Fig. 3

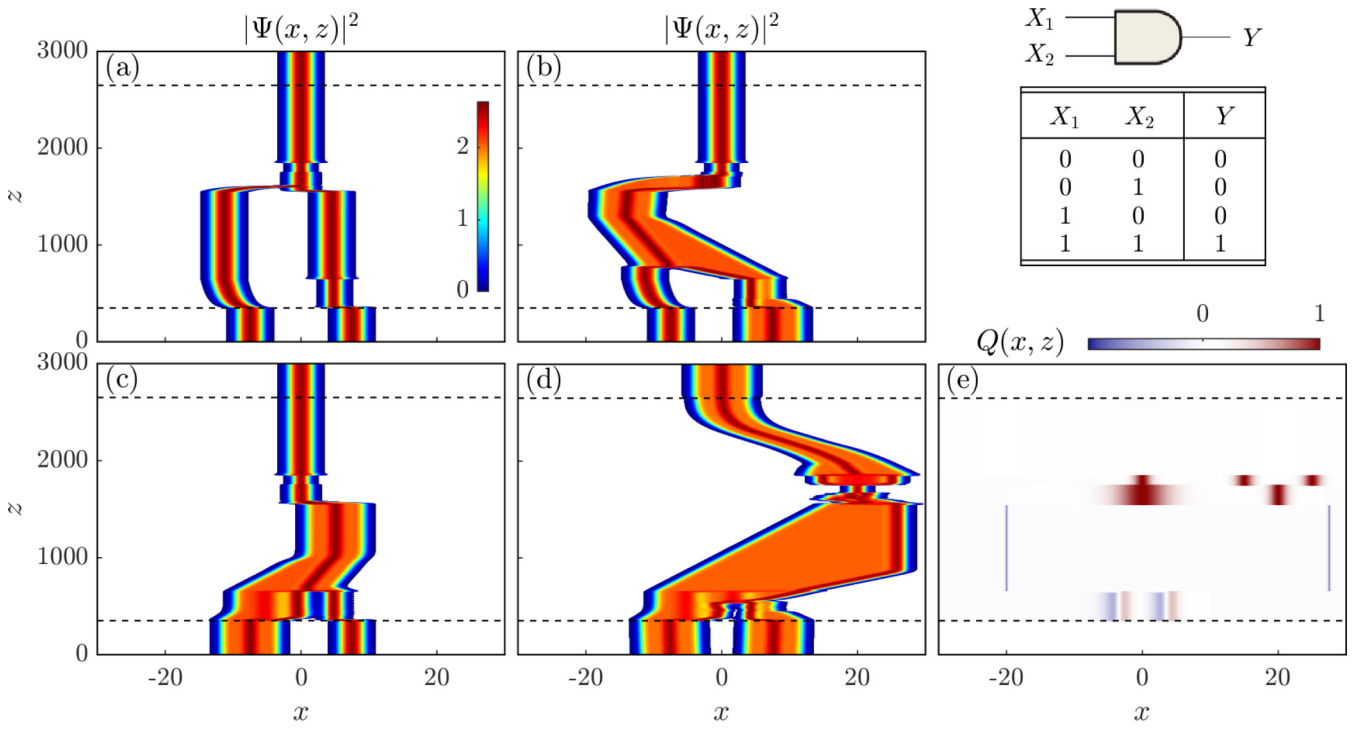

X_1	X_2	Y
0	0	0
0	1	0
1	0	0
1	1	1

FIG. 3. Truth table for a two-input AND gate and its implementation on the dissipative soliton bits due to externally applied potential $Q(x, z)$ with the parameters (6): (a)–(d) soliton envelope intensity plots for all four input combinations and (e) plot of control potential.

is performed using the potential (2) with the parameters

$$\begin{aligned} a_i &\in \{350, 650, 1550, 1750, 1850\},\\ b_i &\in \{650, 1550, 1750, 1850, 2650\},\\ q_1(x) &= \frac{\tanh(x+3.5)}{\cosh(x+3.5)} + \frac{\tanh(x-3.5)}{\cosh(x-3.5)},\\ q_2(x) &= -\mathrm{sech}(10x+200) - \mathrm{sech}(10x-275),\\ q_3(x) &= \mathrm{sech}\left(\frac{x}{3}\right) + \mathrm{sech}(x-20),\\ q_4(x) &= \mathrm{sech}(x) + \mathrm{sech}(x-15) + \mathrm{sech}(x-25),\\ q_5(x) &= \frac{1}{20}\mathrm{sech}\left(\frac{x}{10}\right) + \frac{1}{25}\mathrm{sech}\left(\frac{x}{5}\right). \end{aligned} \tag{6}$$

Figures 3(a)–3(d) show the two-dimensional intensity plots $|\Psi(x, z)|^2$ representing the waveform evolution for all possible combinations of two input pulses, where the peaks of the left and right input pulses are respectively located at the points $x = -7.5$ and $x = 7.5$, while the output pulse is centered around the point $x = 0$. In each of the four cases presented in Figs. 3(a)–3(d), the waveform evolution of two input pulses is controlled by the potential (2) with the same parameters (6) whose two-dimensional spatial distribution $Q(x, z)$ is plotted in Fig. 3(e). This control potential selectively transits the pairs of input pulses to a certain single pulse in five stages ($N = 5$), leading to the different output pulses depending on a particular combination of input pulses. In particular, Fig. 3(a) shows the controllable evolution of two plain pulses to one plain pulse that corresponds to the first row in the truth table for a two-input AND gate presented in Fig. 3. Moreover, in Figs. 3(b) and 3(c) we see how two different pairs comprised of the plain and composite pulses are transited to the plain pulse. These two transitions correspond to the second and third rows in the truth table in Fig. 3. Finally, in Fig. 3(d) the last possible input combination of two composite pulses is transited to the composite pulse corresponding to the fourth row in the truth table in Fig. 3.

In other words, in Figs. 3(a)–3(d) we demonstrate the four basic rules for multiplying the soliton bits, where each multiplication is represented by the controllable interaction of two-input pulses induced by the external potential (2) with (6). Looking at Eqs. (6) and Fig. 3(e), we see that this potential is chosen to perform the rules for five control manipulations over soliton waveforms. First of all we apply $q_1(x)$ from Eqs. (6) to perturb the waveforms of input pulses selectively, i.e., accounting for the soliton bit combination of input pulses. Then we apply the second manipulation $q_2(x)$ to release the selectively perturbed waveforms as well as to prevent the wide spreading of released waveforms along the transverse direction. As a result, the perturbed waveform of two input composite pulses is significantly moved along the positive direction of the x axis [Fig. 3(d)], while for other input pulses the waveforms are slightly shifted along the positive direction of the x axis [Fig. 3(c)] or are shifted in the opposite direction [Figs. 3(a) and 3(b)], leading to the spatial separation of waveforms along the x axis. Further, we apply $q_3(x)$ to transit all the transformed and shifted waveforms to the plain pulses. However, the waveform evolved from two composite pulses is transited to the plain pulse whose peak is located at the point $x = 20$ [Fig. 3(d)], while other waveforms are transited to the plain pulse with a peak

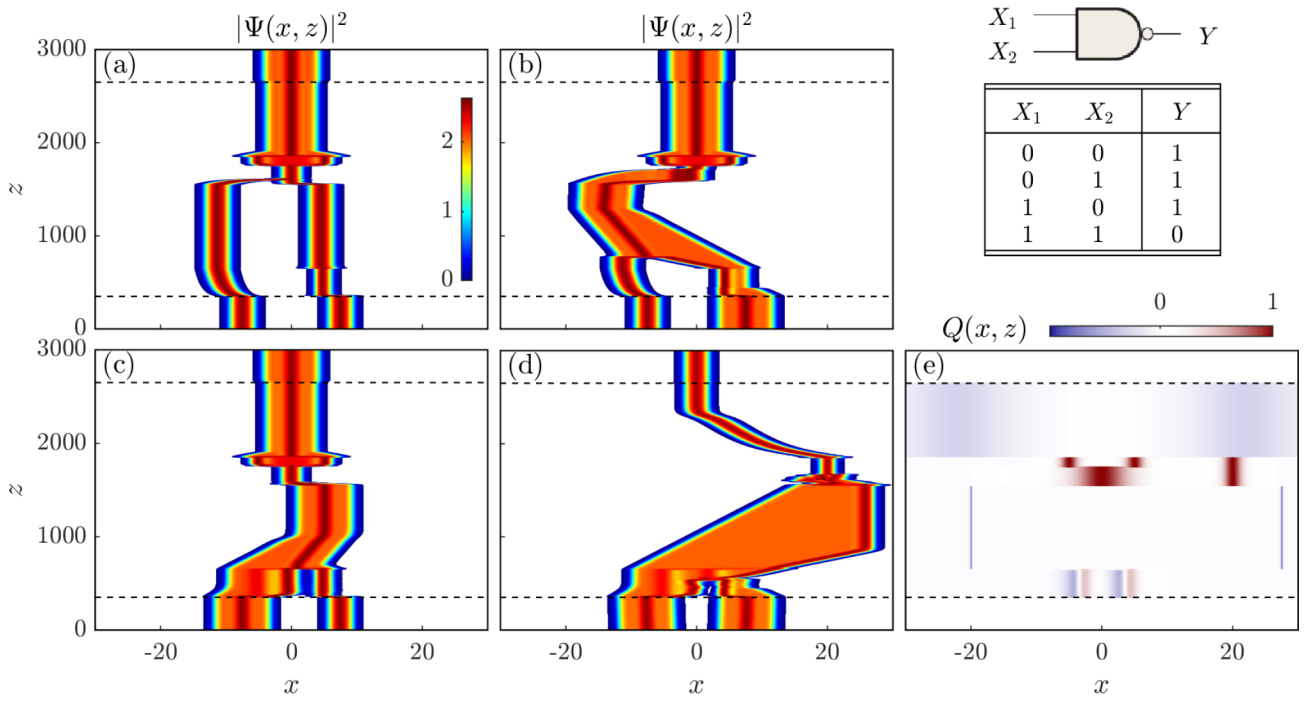

X_1	X_2	Y
0	0	1
0	1	1
1	0	1
1	1	0

FIG. 4. Truth table for a two-input NAND gate and its implementation on the dissipative soliton bits due to externally applied potential $Q(x, z)$ with the parameters (6), where the last two control manipulations are replaced by Eqs. (7): (a)–(d) soliton envelope intensity plots for all four input combinations and (e) plot of control potential.

at $x = 0$ [Figs. 3(a)–3(c)]. The fourth control manipulation $q_4(x)$ is applied to transit the plain pulse centered around the point $x = 20$ to the composite pulse [Fig. 3(d)] and to prevent the lateral shift of the plain pulses centered at the point $x = 0$ [Figs. 3(a)–3(c)]. The last manipulation $q_5(x)$ is applied to shift the composite pulse at the point $x = 0$ [Fig. 3(d)], while the transverse positions of the plain pulses are not changed because they have already been centered at the point $x = 0$ [Figs. 3(a)–3(c)]. Thus, we complete the implementation of the two-input AND gate on the dissipative soliton bits.

Having replaced the last two control manipulations $q_4(x)$ and $q_5(x)$ in Eqs. (6) by

$$\begin{aligned} q_4(x) &= \mathrm{sech}(x+5) + \mathrm{sech}(x-5) + \mathrm{sech}(x-20), \\ q_5(x) &= \frac{1}{25}\left[\mathrm{sech}(x) + \mathrm{sech}\left(\frac{x}{5}\right)\right] \\ &\quad - \frac{3}{10}\left[\mathrm{sech}\left(\frac{x+22}{5}\right) + \mathrm{sech}\left(\frac{x-22}{5}\right)\right], \end{aligned} \tag{7}$$

we get the appropriate potential to implement a two-input NAND gate whose operation is opposite to that of the AND gate in terms of the output level. As it is summarized in the truth table presented in Fig. 4, for a two-input NAND gate, output Y is low only when inputs X_1 and X_2 are high; Y is high when either X_1 or X_2 is low or when both X_1 and X_2 are low. We demonstrate the implementation of the two-input NAND gate on the dissipative soliton bits in Figs. 4(a)–4(d), where each graph shows the evolution of the soliton intensity $|\Psi(x, z)|^2$ under the influence of the control potential (2) with the same parameters (6) used to implement the AND gate except for the last two manipulations $q_4(x)$ and $q_5(x)$, which we now take in the form of Eqs. (7). The two-dimensional spatial distribution of this potential $Q(x, z)$ is plotted in Fig. 4(e).

We see that the graphs presented in Figs. 4(a)–4(d) are similar to those shown in Figs. 3(a)–3(d), respectively. Moreover, the first three control manipulations are identical for both gates. However, we apply the fourth control manipulation $q_4(x)$ to transit the plain pulses centered around the point $x = 0$ to the composite pulse [Figs. 4(a)–4(c)] and to prevent the waveform change of the plain pulse centered at the point $x = 20$ [Fig. 4(d)]. The last manipulation $q_5(x)$ is applied to shift the plain pulse laterally from the point $x = 20$ to the point $x = 0$ [Fig. 4(d)] and save the waveforms of composite pulses already centered at the point $x = 0$ [Figs. 4(a)–4(c)]. That implements the two-input NAND gate based on the dissipative solitons.

C. The OR and NOR gates

Below we demonstrate the implementation of an OR gate with two inputs in the framework of the model (1)–(3) supporting the coexisting plain and composite pulses presented in Fig. 1. An OR gate produces a high level on the output when either of the inputs is high. The output is low only when both of the inputs are low. The operation of a two-input OR gate is described in the truth table presented in Fig. 5, where the inputs are labeled X_1 and X_2 and the output is labeled Y. The implementation of an OR gate with two dissipative soliton inputs is demonstrated in Figs. 5(a)–5(d), where each graph shows the intensity plot $|\Psi(x, z)|^2$ that represents the possible evolution of two input pulses into a single output under the

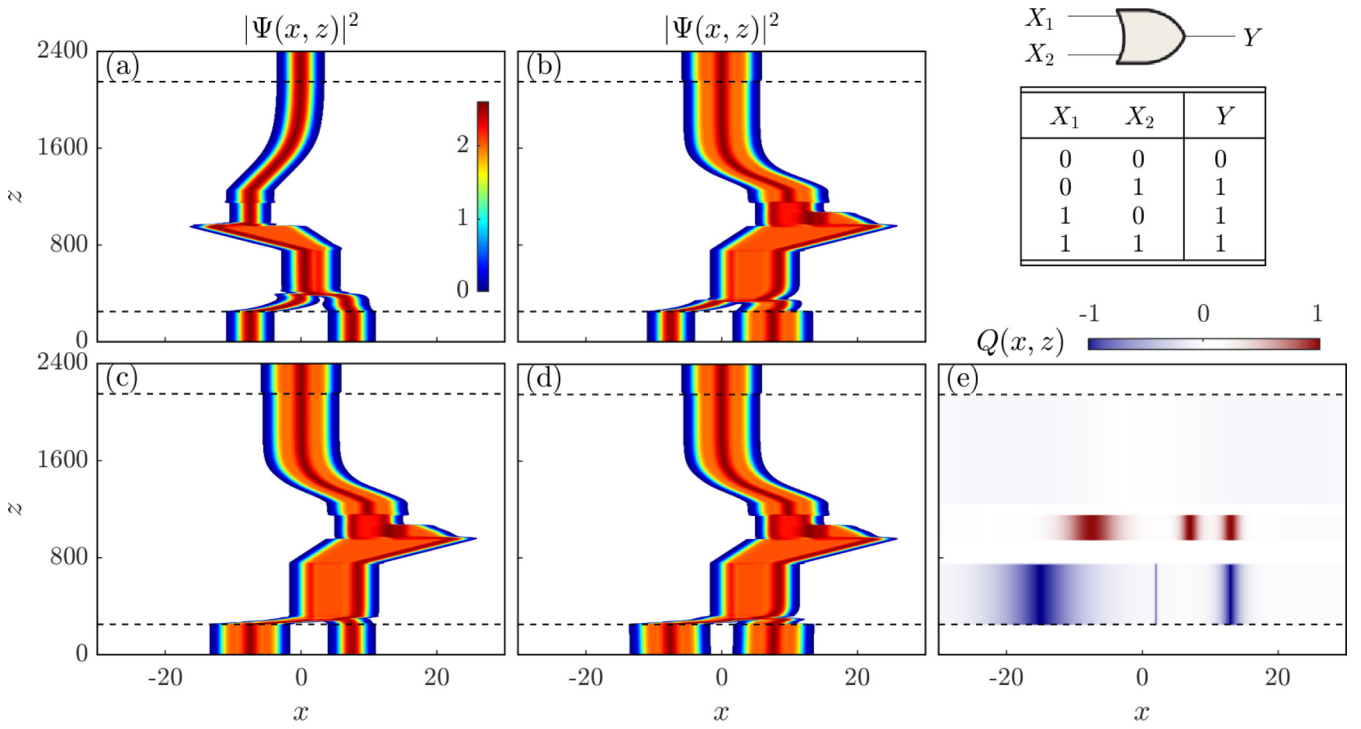

FIG. 5. Truth table for a two-input OR gate and its implementation on the dissipative soliton bits due to externally applied potential $Q(x, z)$ with the parameters (8): (a)–(d) soliton envelope intensity plots for all four input combinations and (e) plot of control potential.

control of the potential (2) with the parameters

$$a_i \in \{250, 950, 1250\}, \quad b_i \in \{750, 1150, 2150\},$$

$$q_1(x) = -\text{sech}\left(\frac{x+15}{4}\right) - \text{sech}(x-13) - \text{sech}(10x-20),$$

$$q_2(x) = \text{sech}\left(\frac{x+7.5}{3}\right) + \text{sech}(x-7) + \text{sech}(x-13),$$

$$q_3 = \frac{1}{20}\left[\text{sech}\left(\frac{x}{5}\right) - \text{sech}\left(\frac{x+19}{10}\right) - \text{sech}\left(\frac{x-19}{10}\right)\right]. \quad (8)$$

Again, we stress that the two-input OR gate presented in Figs. 5(a)–5(d) has been implemented due to the proper choice of parameters (8) of the potential (2). The two-dimensional distribution of the potential $Q(x, z)$ with the parameters (8) is plotted in Fig. 5(e). When applied this potential induces the plain pulse output only when both inputs are the plain pulses as shown in Fig. 5(a). On the other hand, when either of the two inputs (including both of them) is the composite pulse, the output is the composite pulse [Figs. 5(b)–5(d)]. Therefore, looking at the plain and composite pulses as Boolean variables whose values are respectively either binary 0 or binary 1, we conclude that Figs. 5(a)–5(d) also implement the basic rules for Boolean addition.

The applied potential (2) with the parameters (8) performs the OR gate in three control stages, which are shown in Fig. 5(e). First of all, we apply $q_1(x)$ to transit four different pairs of input pulses to so-called moving pulses [14,62]. The asymmetrical profile of $q_1(x)$ is properly chosen to transit two input plain pulses to the moving pulse with a transverse drift along the negative direction of the x axis [Fig. 5(a)], while all other input combinations are transited to the moving pulse with the opposite transverse drift [Figs. 5(b)–5(d)]. The second stage succeeds the first one after some delay. During that delay the moving pulses are released from the potential influence that allows them to freely travel along the x axis as seen in Figs. 5(a)–5(d). At some moment the pulses traveling in opposite directions get sufficient spatial separation between them, which allows us to apply the potential $q_2(x)$ to transit the left-shifted waveform to the plain pulse [Fig. 5(a)] while the right-shifted waveforms are transited to the composite pulse [Figs. 5(b)–5(d)]. Finally, having applied the weak potential $q_3(x)$, we symmetrically arrange the plain and composite pulses around the point $x = 0$ and complete the implementation of the OR gate.

It is logical to note that if during the second stage we transit the left-shifted (right-shifted) waveform to the composite (plain) pulse we implement a two-input NOR gate, which is the same as the OR except the output is inverted (see the truth table in Fig. 6). Therefore, we replace the potential parameter $q_2(x)$ in Eqs. (8) by

$$q_2(x) = \text{sech}(x+10.5) + \text{sech}(x+4.5) + \text{sech}\left(\frac{x-7.5}{3}\right) \quad (9)$$

to get the potential suitable for the implementation of a two-input NOR gate on dissipative soliton bits. The implementation of this NOR gate is shown in Fig. 6. All plots in Fig. 6 are similar to those in Fig. 5. Indeed, the graphs in Figs. 6(a)–6(d)

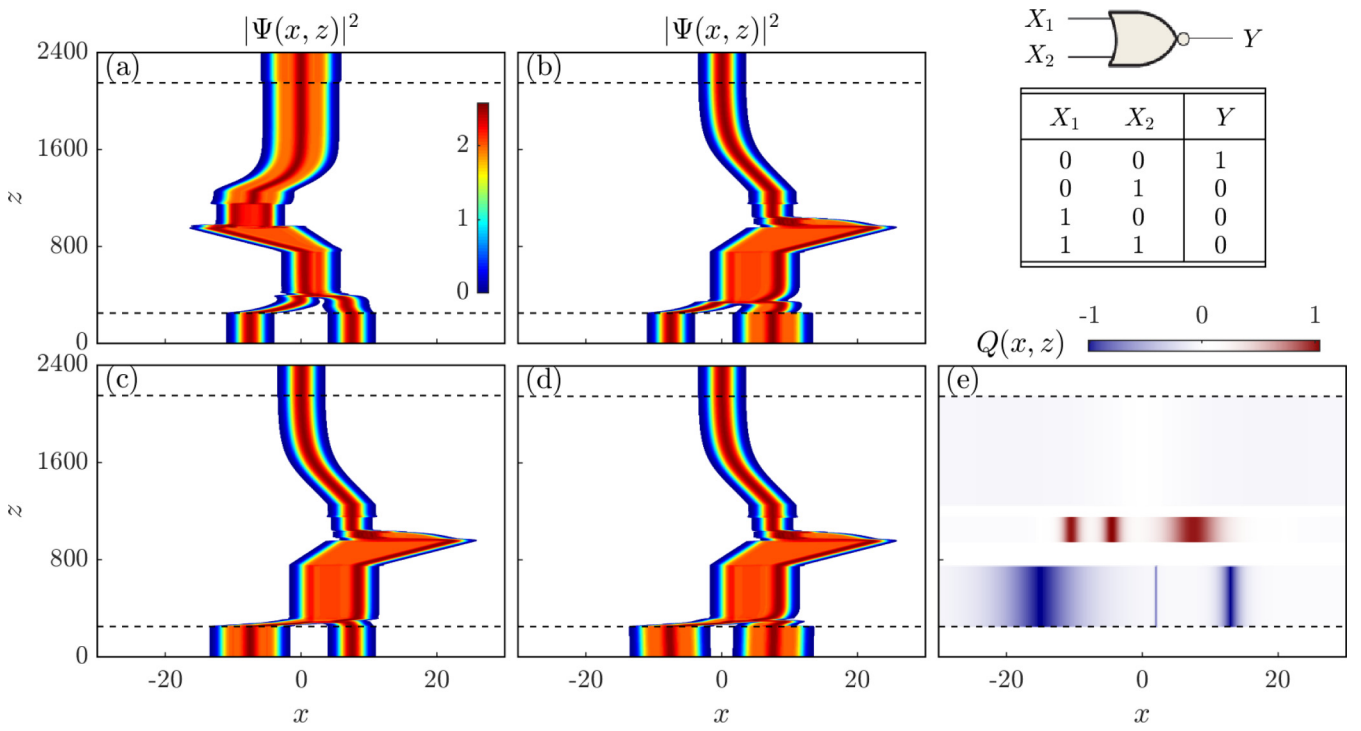

FIG. 6. Truth table for a two-input NOR gate and its implementation on the dissipative soliton bits due to externally applied potential $Q(x, z)$ with the parameters (8), where the second control manipulation is replaced by Eq. (9): (a)–(d) soliton envelope intensity plots for all four input combinations and (e) plot of control potential.

show the two-dimensional intensity plots $|\Psi(x, z)|^2$, while Fig. 6(e) depicts the spatial distribution of the control potential $Q(x, z)$ with the parameters (8), where the parameter $q_2(x)$ is replaced by Eq. (9).

D. The XOR and XNOR gates

Finally, we discuss the implementation of an XOR gate, which performs modulo-2 addition. Its operation is summarized in the truth table shown in Fig. 7. To implement an XOR gate on dissipative soliton bits we again employ the controllable model (1)–(3) supporting the same plain and composite pulses (Fig. 1) as we used above. In Figs. 7(a)–7(d) we demonstrate the four possible input combinations and the resulting outputs for the XOR gate implemented on the plain and composite pulses, where in each graph we plot the evolution of soliton intensities $|\Psi(x, z)|^2$. These simulations of the XOR gate have been performed using the control potential (2) with the parameters specified as

$$a_i \in \{250, 950, 1150\}, \quad b_i \in \{650, 1050, 1750\},$$

$$q_1(x) = -\mathrm{sech}(10x) - \mathrm{sech}\left(\frac{x+15}{4}\right) - \mathrm{sech}\left(\frac{x-15}{4}\right),$$

$$q_2(x) = \mathrm{sech}(x+16) + \mathrm{sech}(x+10) + \mathrm{sech}(x) + \mathrm{sech}(x-10) + \mathrm{sech}(x-16),$$

$$q_3 = \frac{1}{20}\left[\mathrm{sech}\left(\frac{x}{5}\right) - \mathrm{sech}\left(\frac{x+19}{10}\right) - \mathrm{sech}\left(\frac{x-19}{10}\right)\right]. \tag{10}$$

The two-dimensional spatial distribution of this control potential is illustrated in Fig. 7(e).

Since the high output level occurs in an XOR gate only when the inputs are at opposite levels, we first apply the potential $q_1(x)$ that selectively transits the pairs of input pulses depending on whether the same or different pulses are launched to the gate. Indeed, two plain pulses [Fig. 7(a)] as well as two composite pulses [Fig. 7(d)] are transited by the potential (2) with the parameters (10) to the plain pulse, while the combinations of plain-composite [Fig. 7(b)] and composite-plain [Fig. 7(c)] pulses are transited to the moving pulses with positive and negative drifts along the x axis, respectively. Between the first and second control manipulations is some lag leading to the significant displacements of moving pulses along the x axis as illustrated in Figs. 7(b) and 7(c). After that, we apply the potential $q_2(x)$ to transit the shifted moving pulses to the composite pulse [Figs. 7(b) and 7(c)] and keep the plain pulses unchanged [Figs. 7(a) and 7(d)]. Finally, we apply the weak potential $q_3(x)$ to arrange all the pulses around the point $x = 0$.

Thus, we has completed the implementation of the XOR gate and found a simple way to implement the XNOR gate whose outputs are opposite to those of the XOR gate, as summarized in the truth table for an XNOR gate shown in Fig. 8. In fact, to implement the XNOR gate we again use the potential (2) with the parameters (10) except for the last two control manipulations, which are now chosen in the form

$$q_2(x) = \mathrm{sech}(2x+6) + \mathrm{sech}(2x-6) + \mathrm{sech}\left(\frac{x+13}{3}\right) + \mathrm{sech}\left(\frac{x-13}{3}\right),$$

$$q_3(x) = \frac{1}{20}\mathrm{sech}(x) - \mathrm{sech}\left(\frac{x+15}{2.5}\right) - \mathrm{sech}\left(\frac{x-15}{2.5}\right). \tag{11}$$

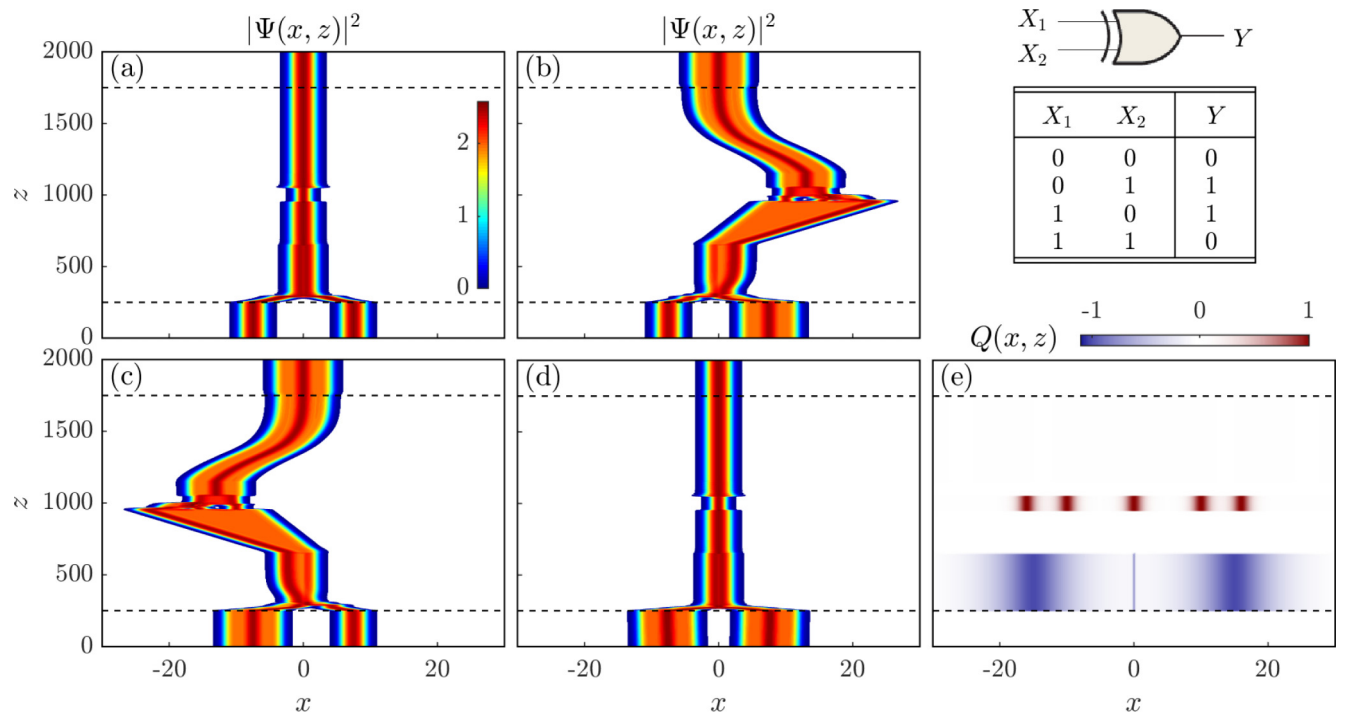

X_1	X_2	Y
0	0	0
0	1	1
1	0	1
1	1	0

FIG. 7. Truth table for an exclusive-OR (XOR) gate and its implementation on the dissipative soliton bits due to externally applied potential $Q(x, z)$ with the parameters (10): (a)–(d) soliton envelope intensity plots for all four input combinations and (e) plot of control potential.

Having performed the first stage and having waited for some lag between the first and second manipulations, we proceed to the second stage. During the second stage we now apply the potential $q_2(x)$ from Eqs. (11) to transit the plain pulses to the composite pulse [Figs. 8(a) and 8(d)] and the laterally shifted (moving) pulses to the plain pulse [Figs. 8(b) and 8(c)]. Finally, we apply the potential $q_3(x)$ from Eqs. (11) to center the shifted pulses with respect to the

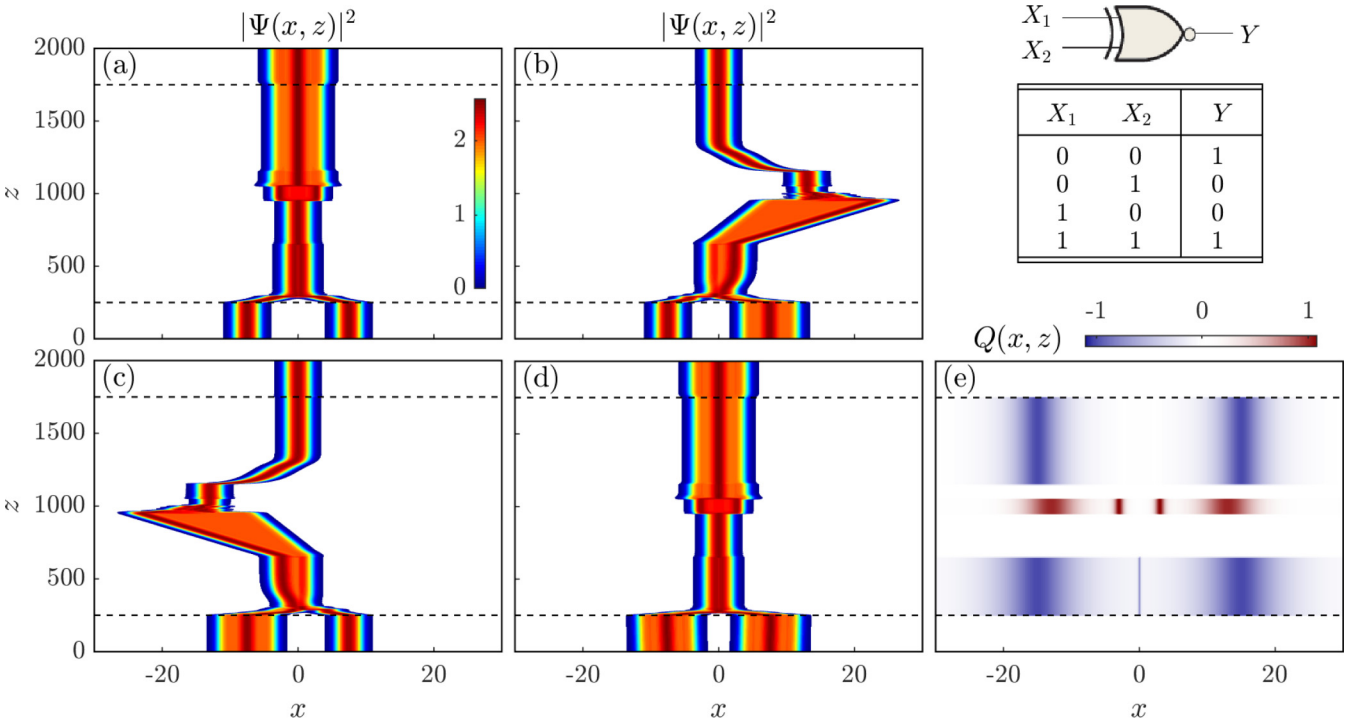

X_1	X_2	Y
0	0	1
0	1	0
1	0	0
1	1	1

FIG. 8. Truth table for an exclusive-NOR (XNOR) gate and its implementation on the dissipative soliton bits due to externally applied potential $Q(x, z)$ with the parameters (10), where the last two control manipulations are replaced by Eqs. (11): (a)–(d) soliton envelope intensity plots for all four input combinations and (e) plot of control potential.

point $x = 0$ and complete the implementation of XNOR gate. We replace the last control manipulation $q_3(x)$ to move the shifted plain pulses [Figs. 7(b) and 7(c)] faster than we moved the corresponding composite pulses in Fig. 7.

IV. CONCLUSION

In our numerical simulations presented in Figs. 2–8 we have demonstrated the implementation of basic logic gates, where two logic levels are represented by two stationary dissipative solitons with distinguished waveforms and spectra. The simulations have been carried out in the framework of the one-dimensional cubic-quintic CGLE with a potential term (1). This equation accounts for the most important features of dissipative solitons while admitting the existence of a wide range of sophisticated solutions. That makes it one of the basic mathematical models of dissipative solitons in many applications. In particular, Eq. (1) admits the coexistence of two stationary solutions in the form of plain and composite pulses (Fig. 1), which were used here to represent the low and high logic levels, respectively. Moreover, Eq. (1) contains the external potential $Q(x, z)$, which we applied to control the evolution of solitons within the system. In fact, the potential has a vital impact on the soliton dynamics and plays the most important role in the implementation of logic gates. In each simulation we applied the potential (2) with some parameters properly chosen to implement a given logic gate. These particular parameters were given in Eqs. (5)–(11), where the transverse profiles $q_i(x)$ were chosen in the form of combinations of scaled sech(x) functions. However, they contain all the significant properties of the potentials suitable to implement the logic gates. In general, an appropriate potential implements a logic gate in three basic control stages. This operation can be stated as follows.

(i) The potential selectively transforms and shifts along the transverse direction the pairs of input pulses depending on their input combinations. In other words, during the first stage we perform the transverse spatial selection of input solitons, i.e., different combinations of input pulses get different lateral shifts.

(ii) The potential transits each spatially separated pulse to the proper output. During the second stage some of the pulses can also be shifted along the transverse direction.

(iii) The potential gradually performs a lateral shift of the output pulses to arrange all the outputs around the same point. We should note that each of these stages can consist of one or several particular control manipulations. For example, the first stage for all the gates discussed here (Figs. 2–8) consists of two control manipulations. For the AND (Fig. 2) and NAND (Fig. 3) gates the first stage has been performed by two functions $q_1(x)$ and $q_2(x)$ from Eqs. (6), but the same stage of all other gates (Figs. 4–8) has been performed by the corresponding functions $q_1(x)$ and subsequent control manipulations with zero transverse functions as shown in Figs. 4(e)–8(e). On the other hand, the third stage for each of the logic gates has been performed by a single control manipulation. For the AND and NAND gates it is the function $q_5(x)$ in Eqs. (6) and (7), while for the other gates it is the function $q_3(x)$ in Eqs. (8)–(11), respectively.

In this paper we have demonstrated a numerical implementation of the basic logic gates with two inputs applying external potentials to get control over soliton waveforms. In particular, we have found the potentials which allow us to get the proper output soliton waveforms depending on a given input. Due to our numerical simulations, we have shown that such potentials should contain three vital control manipulations over input pulses, i.e., transverse spatial selection, waveform transition, and output arrangement, as summarized above.

In our simulations we have used the normalized model (1) written in dimensionless coordinates. It allows us to consider the implementation of logic gates in various physical systems supporting stationary dissipative solitons. Moreover, these general simulations can be used to estimate some operation characteristics of logic gates implemented in a given physical system. In particular, for the aforementioned example with a planar nonlinear magneto-optic waveguide, the longitudinal coordinate z is measured in Rayleigh lengths, which allows us to estimate the propagation time of soliton bits through the logic gates. According to Figs. 2–8, we see that the operation time of the demonstrated logic gates varies from 700 Rayleigh lengths for the NOT gate (Fig. 2) to 2300 Rayleigh lengths for the AND and NAND gates (Figs. 3 and 4). Since our main goal is the demonstration of logic gates implemented on stationary dissipative solitons, we consider the typical logic gate extension of 2000 Rayleigh lengths, which is enough at this stage of our study. Such questions as optimization of logic gate characteristics and how they depend on losses, diffusion, and nonlinearity are subjects left for further study.

Traditionally, digital electronics is built on universal NAND gates, whose combinations can be used to produce any logic function. However, in this case, we have a planar technology, where switching between pulses across tracks is difficult. Therefore, we have considered various logic gates implemented in the planar form.

This approach can also be used to implement other logic gates with two or more inputs as well as to model such optical devices as splitters, demultiplexers, cellular automata, etc., where the dissipative solitons are employed as logic levels (bits). Moreover, the ideas discussed here can be useful for experimental studies on dissipative optical solitons.

ACKNOWLEDGMENT

This work was supported by Jilin University, China.

[1] E. Picholle, C. Montes, C. Leycuras, O. Legrand, and J. Botineau, Observation of Dissipative Superluminous Solitons in a Brillouin Fiber Ring Laser, Phys. Rev. Lett. **66**, 1454 (1991).

[2] E. V. Vanin, A. I. Korytin, A. M. Sergeev, D. Anderson, M. Lisak, and L. Vázquez, Dissipative optical solitons, Phys. Rev. A **49**, 2806 (1994).

[3] *Dissipative Solitons*, edited by N. Akhmediev and A. Ankiewicz (Springer, Berlin, 2005).

[4] *Dissipative Solitons: From Optics to Biology and Medicine*, edited by N. Akhmediev and A. Ankiewicz (Springer, Berlin, 2008).

[5] A. Liehr, *Dissipative Solitons in Reaction Diffusion Systems* (Springer, Berlin, 2013).

[6] M. C. Cross and P. C. Hohenberg, Pattern formation outside of equilibrium, Rev. Mod. Phys. **65**, 851 (1993).

[7] I. S. Aranson and L. Kramer, The world of the complex Ginzburg-Landau equation, Rev. Mod. Phys. **74**, 99 (2002).

[8] V. García-Morales and K. Krischer, The complex Ginzburg-Landau equation: An introduction, Contemp. Phys. **53**, 79 (2012).

[9] N. Akhmediev and A. Ankiewicz, in *Dissipative Solitons* (Ref. [3]), pp. 1–17.

[10] B. A. Malomed, Evolution of nonsoliton and "quasi-classical" wavetrains in nonlinear Schrödinger and Korteweg–de Vries equations with dissipative perturbations, Physica D **29**, 155 (1987).

[11] B. A. Malomed and A. A. Nepomnyashchy, Kinks and solitons in the generalized Ginzburg-Landau equation, Phys. Rev. A **42**, 6009 (1990).

[12] S. Fauve and O. Thual, Solitary Waves Generated by Subcritical Instabilities in Dissipative Systems, Phys. Rev. Lett. **64**, 282 (1990).

[13] W. van Saarloos and P. C. Hohenberg, Fronts, pulses, sources and sinks in generalized complex Ginzburg-Landau equations, Physica D **56**, 303 (1992).

[14] V. V. Afanasjev, N. Akhmediev, and J. M. Soto-Crespo, Three forms of localized solutions of the quintic complex Ginzburg-Landau equation, Phys. Rev. E **53**, 1931 (1996).

[15] W. H. Renninger, A. Chong, and F. W. Wise, Dissipative solitons in normal-dispersion fiber lasers, Phys. Rev. A **77**, 023814 (2008).

[16] R. J. Deissler and H. R. Brand, Periodic, Quasiperiodic, and Chaotic Localized Solutions of the Quintic Complex Ginzburg-Landau Equation, Phys. Rev. Lett. **72**, 478 (1994).

[17] J. M. Soto-Crespo, N. Akhmediev, and A. Ankiewicz, Pulsating, Creeping, and Erupting Solitons in Dissipative Systems, Phys. Rev. Lett. **85**, 2937 (2000).

[18] N. Akhmediev, J. M. Soto-Crespo, and G. Town, Pulsating solitons, chaotic solitons, period doubling, and pulse coexistence in mode-locked lasers: Complex Ginzburg-Landau equation approach, Phys. Rev. E **63**, 056602 (2001).

[19] J. M. Soto-Crespo, N. Akhmediev, and K. S. Chiang, Simultaneous existence of a multiplicity of stable and unstable solitons in dissipative systems, Phys. Lett. A **291**, 115 (2001).

[20] S. T. Cundiff, J. M. Soto-Crespo, and N. Akhmediev, Experimental Evidence for Soliton Explosions, Phys. Rev. Lett. **88**, 073903 (2002).

[21] O. Descalzi, C. Cartes, J. Cisternas, and H. R. Brand, Exploding dissipative solitons: The analog of the Ruelle-Takens route for spatially localized solutions, Phys. Rev. E **83**, 056214 (2011).

[22] W. Chang, J. M. Soto-Crespo, P. Vouzas, and N. Akhmediev, Extreme amplitude spikes in a laser model described by the complex Ginzburg-Landau equation, Opt. Lett. **40**, 2949 (2015).

[23] W. Chang, J. M. Soto-Crespo, P. Vouzas, and N. Akhmediev, Spiny solitons and noise-like pulses, J. Opt. Soc. Am. B **32**, 1377 (2015)

[24] J. M. Soto-Crespo, N. Devine, and N. Akhmediev, Dissipative solitons with extreme spikes: Bifurcation diagrams in the anomalous dispersion regime, J. Opt. Soc. Am. B **34**, 1542 (2017).

[25] N. N. Akhmediev, A. Ankiewicz, and J. M. Soto-Crespo, Multisoliton Solutions of the Complex Ginzburg-Landau Equation, Phys. Rev. Lett. **79**, 4047 (1997).

[26] D. Turaev, A. G. Vladimirov, and S. Zelik, Chaotic bound state of localized structures in the complex Ginzburg-Landau equation, Phys. Rev. E **75**, 045601(R) (2007).

[27] O. Descalzi, H. R. Brand, and J. Cisternas, Hysteretic behavior of stable solutions at the onset of a weakly inverted instability, Physica A **371**, 41 (2006).

[28] J. M. Soto-Crespo and N. Akhmediev, Composite solitons and two-pulse generation in passively mode-locked lasers modeled by the complex quintic Swift-Hohenberg equation, Phys. Rev. E **66**, 066610 (2002).

[29] V. Achilleos, A. R. Bishop, S. Diamantidis, D. J. Frantzeskakis, T. P. Horikis, N. I. Karachalios, and P. G. Kevrekidis, Dynamical playground of a higher-order cubic Ginzburg-Landau equation: From orbital connections and limit cycles to invariant tori and the onset of chaos, Phys. Rev. E **94**, 012210 (2016).

[30] H. Sakaguchi, D. V. Skryabin, and B. A. Malomed, Stationary and oscillatory bound states of dissipative solitons created by third-order dispersion, Opt. Lett. **43**, 2688 (2018).

[31] I. M. Uzunov, Z. D. Georgiev, and T. N. Arabadzhiev, Transitions of stationary to pulsating solutions in the complex cubic-quintic Ginzburg-Landau equation under the influence of nonlinear gain and higher-order effects, Phys. Rev. E **97**, 052215 (2018).

[32] S. V. Gurevich, C. Schelte, and J. Javaloyes, Impact of high-order effects on soliton explosions in the complex cubic-quintic Ginzburg-Landau equation, arXiv:1902.04978.

[33] A. Boardman, L. Velasco, and P. Egan, in *Dissipative Solitons* (Ref. [3]), pp. 19–37.

[34] A. D. Boardman and L. Velasco, Gyroelectric cubic-quintic dissipative solitons, IEEE J. Sel. Top. Quantum Electron. **12**, 388 (2006).

[35] S. Sugavanam, N. Tarasov, S. Wabnitz, and D. V. Churkin, Ginzburg-Landau turbulence in quasi-CW Raman fiber lasers, Laser Photon. Rev. **9**, L35 (2015).

[36] B. A. Malomed, Solitary pulses in linearly coupled Ginzburg-Landau equations, Chaos **17**, 037117 (2007).

[37] O. Descalzi and H. R. Brand, Interaction of exploding dissipative solitons, Eur. Phys. J. B **88**, 219 (2015).

[38] O. Descalzi and H. R. Brand, Collisions of non-explosive dissipative solitons can induce explosions, Chaos **28**, 075508 (2018).

[39] J. Javaloyes, Cavity Light Bullets in Passively Mode-Locked Semiconductor Lasers, Phys. Rev. Lett. **116**, 043901 (2016).

[40] C. Schelte, J. Javaloyes, and S. V. Gurevich, Dynamics of temporally localized states in passively mode-locked semiconductor lasers, Phys. Rev. A **97**, 053820 (2018).

[41] B. A. Malomed, *Soliton Management in Periodic Systems* (Springer, Berlin, 2006).

[42] M. Wouters and I. Carusotto, Excitations in a Nonequilibrium Bose-Einstein Condensate of Exciton Polaritons, Phys. Rev. Lett. **99**, 140402 (2007).

[43] E. A. Ostrovskaya, J. Abdullaev, A. S. Desyatnikov, M. D. Fraser, and Y. S. Kivshar, Dissipative solitons and vortices in polariton Bose-Einstein condensates, Phys. Rev. A **86**, 013636 (2012).

[44] Y. Xue and M. Matuszewski, Creation and Abrupt Decay of a Quasistationary Dark Soliton in a Polariton Condensate, Phys. Rev. Lett. **112**, 216401 (2014).

[45] L. A. Smirnov, D. A. Smirnova, E. A. Ostrovskaya, and Y. S. Kivshar, Dynamics and stability of dark solitons in exciton-polariton condensates, Phys. Rev. B **89**, 235310 (2014).

[46] Y. Xue, Y. Jiang, G. Wang, R. Wang, S. Feng, and M. Matuszewski, Creation of stable dark and anti-dark solitons in polariton dyad, Opt. Express **26**, 6267 (2018).

[47] G. I. Stegeman and M. Segev, Optical spatial solitons and their interactions: Universality and diversity, Science **286**, 1518 (1999).

[48] E. Cancellieri, J. K. Chana, M. Sich, D. N. Krizhanovskii, M. S. Skolnick, and D. M. Whittaker, Logic gates with bright dissipative polariton solitons in Bragg cavity systems, Phys. Rev. B **92**, 174528 (2015).

[49] D. Battogtokh and A. Mikhailov, Controlling turbulence in the complex Ginzburg-Landau equation, Physica D **90**, 84 (1996).

[50] J. Xiao, G. Hu, J. Yang, and J. Gao, Controlling Turbulence in the Complex Ginzburg-Landau Equation, Phys. Rev. Lett. **81**, 5552 (1998).

[51] A. Fratalocchi and G. Assanto, Governing soliton splitting in one-dimensional lattices, Phys. Rev. E **73**, 046603 (2006).

[52] J. Holmer, J. Marzuola, and M. Zworski, Soliton splitting by external delta potentials, J. Nonlinear Sci. **17**, 349 (2007).

[53] R. Yang and X. Wu, Spatial soliton tunneling, compression and splitting, Opt. Express **16**, 17759 (2008).

[54] Y.-J. He, B. A. Malomed, F. Ye, and B. Hu, Dynamics of dissipative spatial solitons over a sharp potential, J. Opt. Soc. Am. B **27**, 1139 (2010).

[55] C. Yin, D. Mihalache, and Y. He, Dynamics of two-dimensional dissipative spatial solitons interacting with an umbrella-shaped potential, J. Opt. Soc. Am. B **28**, 342 (2011).

[56] B. Liu, X.-D. He, and S.-J. Li, Continuous emission of fundamental solitons from vortices in dissipative media by a radial-azimuthal potential, Opt. Express **21**, 5561 (2013).

[57] A. D. Boardman and K. Xie, Magneto-optic spatial solitons, J. Opt. Soc. Am. B **14**, 3102 (1997).

[58] B. A. Kochetov, I. Vasylieva, L. A. Kochetova, H.-B. Sun, and V. R. Tuz, Control of dissipative solitons in a magneto-optic planar waveguide, Opt. Lett. **42**, 531 (2017).

[59] B. A. Kochetov and V. R. Tuz, Cascade replication of dissipative solitons, Phys. Rev. E **96**, 012206 (2017).

[60] B. A. Kochetov and V. R. Tuz, Replication of dissipative vortices modeled by the complex Ginzburg-Landau equation, Phys. Rev. E **98**, 062214 (2018).

[61] B. A. Kochetov and V. R. Tuz, Induced waveform transitions of dissipative solitons, Chaos **28**, 013130 (2018).

[62] B. A. Kochetov, Mutual transitions between stationary and moving dissipative solitons, Physica D **393**, 47 (2019).

[63] H. R. Brand and R. J. Deissler, Interaction of Localized Solutions for Subcritical Bifurcations, Phys. Rev. Lett. **63**, 2801 (1989).

[64] B. Liu, Y.-J. He, B. A. Malomed, X.-S. Wang, P. G. Kevrekidis, T.-B. Wang, F.-C. Leng, Z.-R. Qiu, and H.-Z. Wang, Continuous generation of soliton patterns in two-dimensional dissipative media by razor, dagger, and needle potentials, Opt. Lett. **35**, 1974 (2010).

[65] B. Liu and X.-D. He, Continuous generation of "light bullets" in dissipative media by an annularly periodic potential, Opt. Express **19**, 20009 (2011).

[66] S. Cox and P. Matthews, Exponential time differencing for stiff systems, J. Comput. Phys. **176**, 430 (2002).